JOURNAL OF THERMOPHYSICS AND HEAT TRANSFER
Vol. 24, No. 3, July–September 2010

Investigation of the Importance of Convective Heat Transfer on Laser-Induced Heating

R. Mark Rennie* and Eric J. Jumper†
University of Notre Dame, Notre Dame, Indiana 46556
and
Eric C. Marineau‡
Calspan—University at Buffalo Research Center, Buffalo, New York 14225

DOI: 10.2514/1.47657

A simple computational approach is presented that models the laser-induced heating of a flat-plate target, including convective heat transfer for atmospheric flight conditions up to a Mach number of 4. The results of the computational model are shown to compare well with time-resolved experimental measurements of the temperature distribution in laser targets in high-speed flows. The numerical results are nondimensionalized and compared with analytical solutions to determine general guidelines for the conditions in which convective heat transfer can be expected to have a significant effect on laser heating of typical aerospace materials.

Nomenclature

C_f = skin-friction coefficient
C_P = heat capacity
D = target thickness
D_{crit} = critical thickness for slab-heating type of behavior
h = convective-heat-transfer coefficient
I = irradiance
I_0 = irradiance at center of laser spot
k = thermal conductivity
M = Mach number
Pr = Prandtl number
Q_C = heat transfer by conduction
Q_F = heat transfer by convection
Q_L = absorbed heat input from laser
Q_L^* = nondimensional absorbed heat, $Q_L/[2\pi kD(T - T_0)]$
R = recovery factor
Re = Reynolds number
r = radial coordinate
T = temperature
T_f = fluid temperature
T_r = recovery temperature
T_w = wall temperature
T_0 = target initial temperature
T^* = reference temperature for evaluation of boundary-layer parameters
t = time
t_h = time to heat target material to the melting temperature
V = volume
w = Gaussian spot radius
x = streamwise coordinate
x_0 = boundary-layer development length upstream of laser-contact point
z = longitudinal coordinate
α = thermal diffusivity
δ = boundary-layer thickness
ρ = density
σ = nondimensional convective-heat-transfer coefficient, $hw^2/2kD$
τ = nondimensional time, $(4\alpha/w^2)t$

Received 15 October 2009; revision received 6 February 2010; accepted for publication 13 February 2010.

*Research Assistant Professor, Department of Aerospace and Mechanical Engineering. Senior Member AIAA.
†Professor, Department of Aerospace and Mechanical Engineering. Fellow AIAA.
‡Senior Research Scientist. Member AIAA.

I. Introduction

THE presence of an external flow can significantly influence the interaction of a laser beam with a target material. For example, industrial laser-cutting processes typically employ tangential gas jets to reduce material melt-through times [1,2]. In this case, convective heat transfer from the target material is negligible, and the primary effect of the jet is to speed laser penetration by blowing melted material away from the laser-contact point.

For laser-weapon applications against flight vehicles [3–5], higher flow speeds around the target and concomitant higher convective-heat-transfer coefficients mean that convective heat transfer can potentially have a much greater effect on the laser–target interaction. Because of diffraction effects, beam diameters on targets are also significantly larger at the long ranges associated with weapon applications [3,4], resulting in larger heated areas over which heat can be convected away from the target surface. Significant convective heat transfer from the target can impact the performance of a laser system by lengthening target heating times, thereby increasing the time required to track the laser on target.

Recent wind-tunnel measurements of the laser heating of a thin steel plate with and without flow are described in [6]; however, experimental data acquired specifically to evaluate the effect of convective heat transfer on laser–target interactions for realistic flight conditions are rare. Analytical solutions for the heating of solids by high-intensity continuous laser radiation can be found in (for example) [7,8], and computational approaches to the problem are described in [6,9–11]. For the most part, these analytical and computational solutions contain simplifying assumptions that limit their ability to fully model all possible situations; however, they are still useful for determining the most important physics of the laser–target interaction in particular cases. The objective of the present work is to evaluate the importance of convective heat transfer on laser heating of thin targets for realistic flight conditions. A simple numerical approach is presented and validated against experimental data, and it is used in conjunction with analytical solutions to determine the essential physics of the laser–target interaction with convection. Based on these studies, conditions for which convective heat transfer can be expected to significantly impact laser–target interactions against atmospheric flight vehicles are defined.

II. Approach

A. Analytical Solutions

The problem considered here is the heating of a thin sheet by a laser beam with Gaussian irradiance profile in the presence of an external flow, see Fig. 1. The heat-transfer equation for the problem is given by

$$Q_L + Q_C + Q_F = \rho V C_p \frac{\partial T}{\partial t} \tag{1}$$

In Eq. (1), Q_L is the energy absorbed into the target from the laser, and Q_C is the conducted transfer of heat away from the laser beam, including radial and longitudinal (into the material) components. Radiative heat transfer from the target, as well as temperature variations in the circumferential direction around the laser spot, are not included in the current study. To the authors' knowledge, no analytical solution to the full problem exists; however, analytical solutions to simplified cases exist that incorporate the most essential physics of the laser–target interaction over limited ranges of the problem parameters.

1. Source Heating of a Thin Sheet with Convection

An analytical solution to Eq. (1) that includes the effects of convective heat transfer and radial conduction away from a point source is given in [7]. This solution is expanded to the case of a Gaussian source profile in [8]; at the center of the Gaussian profile (i.e., directly under the laser spot), the solution is

$$\frac{1}{Q_L^*} = \int_0^\tau \frac{\mathrm{d}\tau'}{\tau' + 1} e^{-\sigma\tau'} \tag{2}$$

where the following nondimensional parameters are defined:

$$Q_L^* = \frac{Q_L}{2\pi k D(T - T_0)}; \qquad \tau = \frac{4\alpha}{w^2} t; \qquad \sigma = \frac{hw^2}{2kD} \tag{3}$$

The previous solution is for a thermally thin sheet and does not include the effect of longitudinal heat conduction through the sheet in the z direction.

If convective heat transfer is neglected, Eq. (2) reduces to

$$\frac{1}{Q_L^*} = \ell_n(\tau + 1) \tag{4}$$

or

$$\tau = e^{1/Q_L^*} - 1$$

For small values of Q_L^*, radial conduction of heat away from the laser spot is of the same order of magnitude as the heat absorbed from the laser; in this case, heat transfer in the material takes on a steady-state character, and the time τ required to heat the material to the target temperature asymptotically approaches infinity,

$$\tau \to \infty \tag{5}$$

as

$$Q_L^* \to 0$$

As will be shown later, the effect of convection is to increase heat removal from the target, thereby increasing the nondimensional absorbed laser power Q_L^* at which the solution transitions to the steady-state-like behavior given in Eq. (5).

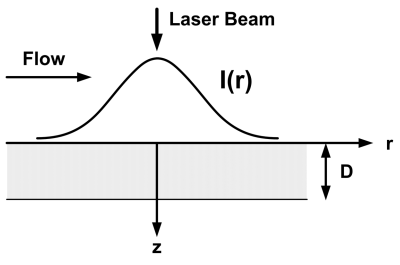

Fig. 1 Schematic of problem.

For larger Q_L^*, Eq. (4) reduces to

$$\tau = \frac{1}{Q_L^*} \tag{6}$$

Physically, Eq. (6) describes the case in which the heat input from the laser is sufficiently large that radial conduction of heat away from the laser spot is negligible over the time required to heat the material surface to the target temperature; in this case, the heat-transfer equation (1) can be approximated as [2]

$$\frac{\partial T}{\partial t} \approx \frac{Q_L}{\rho V C_P} \tag{7}$$

where V is roughly the volume of material directly under the laser beam and is proportional to Dw^2. Integration and nondimensionalization of Eq. (7) gives the same relationship as Eq. (6).

2. Heating of an Infinite Thin Sheet

The previous solution does not model longitudinal conductive heat transfer in the target. In particular, the solution for large Q_L^* [Eq. (6)] assumes constant temperature through the target thickness; in reality, the target will have a significant variation in temperature through its thickness that may impact heating times. An analytical solution for the heating of an infinite thin plate with conductive heat transfer in the z direction is [7]:

$$\frac{1}{Q_L^*} = \tau + \frac{4D^2}{w^2} A(z) - \frac{8D^2}{\pi^2 w^2} \sum_{n=1}^{\infty} \frac{(-1)^n}{n^2} \exp\left(\frac{-w^2 n^2 \pi^2 \tau}{4D^2}\right) \cos\frac{n\pi z}{D} \tag{8}$$

For large times, the final transient term in Eq. (8) decays to zero; the solution then takes the form of a fixed temperature distribution $A(z)$, with the temperature at all points in the target increasing linearly with time at the same rate,

$$\frac{1}{Q_L^*} = \tau + \frac{4D^2}{w^2} A(z) \tag{9}$$

where

$$A(z) = \frac{3(z^2 - D^2)}{6D^2} \tag{10}$$

For laser interactions with atmospheric flight vehicles, material thicknesses are typically small when compared with the beam radius, so that the ratio D^2/w^2 is very small; in this case, the final term in Eq. (9) can also be neglected, giving

$$\tau = \frac{1}{Q_L^*} \tag{11}$$

This is exactly the same solution that was obtained for the previous case in which longitudinal heat transfer was not modeled. It should be noted that this result does not imply that the target will have constant temperature through its thickness; on the contrary, the solution of Eq. (9) shows that the front-to-back temperature variation through the target is reasonably large for realistic cases. Rather, this analysis shows that, for small D^2/w^2, heating of the target is so rapid that there is negligible difference in the time for the front and back of the target to achieve a given temperature.

3. Heating of a Semi-Infinite Slab

For higher absorbed power Q_L, the appropriate boundary conditions for the problem change. As shown in [12], the heating of the target surface in this case can be modeled as a semi-infinite slab subjected to an incident heat flux; an analytical solution for the time to achieve the melting temperature for this case is given by [7,12]

$$t_h = \frac{\pi}{\alpha}\left[\frac{k(T-T_0)}{2I}\right]^2 \tag{12}$$

or, directly under the center of the Gaussian laser spot,

$$t_h = \frac{\pi}{\alpha}\left[\frac{k\pi w^2(T-T_0)}{Q_L}\right]^2 \tag{13}$$

Therefore, for high input power, the melting time t_h switches from the inverse-linear relation in Eq. (6) to the inverse-squared dependence on Q_L, shown in Eq. (13).

4. Summary

The analytical solutions to the problem suggest the existence of three distinct solution domains, each with different dominant heat-transfer mechanisms. First, a low-power domain can be identified in which Q_L is largely balanced by heat transfer away from the laser spot by conduction and convection; in this case, the rate of change of the target temperature becomes small, and heating times become large [Eq. (5)]. At medium powers, radial heat conduction away from the laser becomes negligible, so that the main effect of the laser is to heat the volume of target material directly under the laser spot [Eqs. (6) and (11)]. Finally, at high powers, heat transfer in the target material becomes dominated by longitudinal conduction of heat through the material thickness, and target heating times switch to an inverse-squared dependence on Q_L. The analytical solution that best describes the behavior and physics of a given laser–target interaction depends upon the parameters of the particular situation but primarily upon the absorbed laser power Q_L.

B. Description of Computational Model

The numerical approach was based on the work of [9,10]. Conductive heat transfer was computed using a first-order explicit finite-difference scheme formulated in cylindrical coordinates and assuming axial symmetry about the laser-contact point [13]:

$$Q_{Ci,j} = k\left(\frac{T_{i+1,j} - 2T_{i,j} + T_{i-1,j}}{(\Delta r)^2} + \frac{T_{i+1,j} - T_{i-1,j}}{2r\Delta r} + \frac{T_{i,j+1} - 2T_{i,j} + T_{i,j-1}}{(\Delta z)^2}\right) \tag{14}$$

In Eq. (14), $Q_{Ci,j}$ is the heat conducted into the element $i,\ j$, shown in Fig. 2. Material properties, including thermal conductivity and heat capacity, were assumed to be constant and isotropic. The assumption of constant properties was not considered to be a serious limitation, because the intention of the code was to model a fairly small range of target temperatures associated with typical flight conditions up to the onset of melting; variations in properties for typical aerospace materials over this narrow temperature range are reasonably small.

The laser irradiance was modeled using a Gaussian distribution:

$$I(r) = I_0 \exp\left(\frac{-2r^2}{w^2}\right) \tag{15}$$

The laser heat input Q_L to any finite-difference element was determined by integrating Eq. (15) over the surface area of the element exposed to the laser beam.

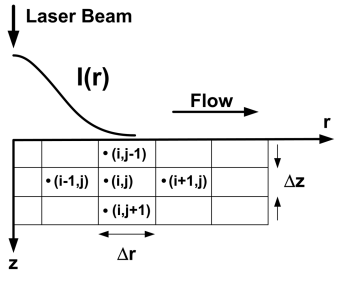

Fig. 2 Schematic of computational domain.

The convective-heat-transfer coefficient was determined using a turbulent boundary-layer skin-friction correlation [9,10,14],

$$h_x = \frac{\rho * C_P U_\infty C_{fx}}{2Pr^{2/3}} \tag{16}$$

where

$$C_{fx} = \frac{0.370}{\log_{10}(Re_x^*)^{2.584}} \tag{17}$$

The asterisked quantities in Eqs. (16) and (17) are evaluated at a reference temperature T^* [14] that lies partway between the wall temperature T_w and the fluid temperature T_f,

$$T^* = 0.5(T_f + T_w) + 0.22(T_r - T_w) \tag{18}$$

where T_r is the recovery temperature:

$$T_r = T_f(1 + 0.2RM^2) \tag{19}$$

In Eq. (19), the recovery factor R was approximated using

$$R = Pr^{1/3} \tag{20}$$

Unlike the laser heat input and the conductive heat-transfer terms, the convective heat transfer does not exhibit axial symmetry about the laser-contact point; rather, it varies in the streamwise direction. However, the radial extent of the region that is significantly heated by the laser is relatively small, so that if the laser-contact point is in a region where the boundary layer is well developed, then the variation in h_x is small over the heated area of the material. As such, a constant value for the convective-heat-transfer coefficient was used for the entire material surface, which was computed at the location of the laser-contact point.

C. Code Validation

Experimental measurements of the laser-induced heating of a flat-plate target, with and without flow, are described in [6]. The measurements were performed in a blowdown supersonic wind tunnel with a 230 mm^2 test section, and the target was a 2.54-mm-thick stainless-steel plate oriented parallel to the flow direction. The target was irradiated with a 1.08 μm wavelength laser beam with a diameter of 4 mm (e^{-2}) and a Gaussian irradiance profile that contacted the target at normal incidence at a point 100 mm downstream of the leading edge of the plate. The flow-on tests were run at a Mach number of $M = 3.75$, with a flow total temperature of 295 K (ambient), a total pressure of 1.1 MPa, and a Reynolds number of 5×10^7/m. The boundary-layer thickness at the laser-beam contact point was measured to be 4 mm. Flow-off and flow-on tests were run at laser powers ranging from 65 to 120 W, giving peak beam irradiances I_0 of 1035 to 1910 W/cm^2. Temperature distributions on the front (i.e, the side of the plate exposed to the laser) and back of the plate were measured using an infrared camera and checked with point measurements using thermocouples. A schematic of the experimental setup is shown in Fig. 3.

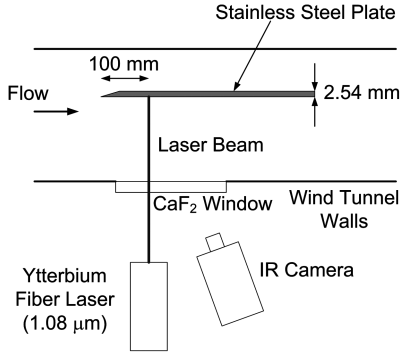

Fig. 3 Wind-tunnel test setup [6] (IR denotes infrared).

The experimental measurements were numerically modeled using the approach described in Sec. II.B. The computational domain was 25 beam radii in diameter and was divided into 200 radial and 10 thickness elements. A time step of 0.005 s was used, which was selected based on the stability analysis equation for the numerical approach [9]:

$$\text{Maximum } \Delta t = \frac{\rho C_P \Delta z^2}{2k} \tag{21}$$

Constant values were used for the thermal conductivity and heat capacity, $k = 22$ W/mK and $C_P = 600$ J/kg/K, which are average values over the experimental temperature range for AISI-304 stainless steel. For the flow-on computations, the effective boundary-layer growth distance was computed using a standard turbulent boundary-layer growth relation [15],

$$\frac{\delta}{x} = \frac{0.16}{Re_x^{*1/7}} \tag{22}$$

where, in Eq. (22), δ was set to the experimentally measured boundary-layer thickness of 4 mm.

Experimentally measured and computed target temperature distributions are compared in Fig. 4 for flow off and in Fig. 5 for flow-on conditions. Generally, the computational model shows very good agreement with the experimental data. The largest differences between the computed and experimental results occur for the target back temperatures; however, accurate modeling of the target back temperatures is not as critical for determining the initiation of target melting, which will occur on the front face, directly under the laser spot. Computed and measured maximum target front-surface temperatures directly under the laser-contact point are summarized in Fig. 6 and show very good agreement.

III. Computational Study

Using the code developed in Sec. II, a computational study was performed to evaluate the importance of convection on laser–target interactions. The study was restricted to situations in which the laser contacts the target away from local stagnation points and in a region in which boundary-layer development is well approximated using the flat-plate convective-heat-transfer correlations incorporated into the numerical model; a schematic of the interaction geometry is shown in Fig. 7. For all cases examined in the study, the boundary-layer development length upstream of the laser-contact point was set at 4 m; this distance is a fairly representative length scale for atmospheric flight vehicles (e.g., wing chord or missile length), and it is long enough for the boundary layer to become fully developed, such that local convective-heat-transfer coefficients, computed using Eq. (16), are nearly constant with x. The scope of the study was limited to flow Mach numbers up to $M = 4$ and flow properties corresponding to atmospheric flight between sea level and 15 km ($\sim$50,000 ft) (Fig. 8). Overall, the parameters of the study were chosen to simulate realistic engagement scenarios in which convective heat transfer might be expected to have a significant effect on laser–target heating interactions.

The focus of the study was determination of the time t_h required for the laser to heat the surface of the target material to the melting point. To achieve a complete burnthrough of the target, an additional amount of energy equal to the latent heat of melting for the target material would still have to be deposited by the laser beam, after which, for the convected-flow cases under consideration here, it is reasonable to assume that the melted target material would be rapidly blown away from the laser-contact point. For typical aerospace materials and engagement parameters, the time required to heat the target to the melting point is still likely to be significantly larger than the additional time needed to melt through the target material, especially if it is noted that the absorptivity of the material is likely to increase dramatically, once melting has been initiated, due to the degradation of polished or reflective surface finishes. Furthermore, as noted in [3], complete burnthrough of the target is not always necessary, because successful engagements can be achieved in some cases by heating the target skin to a failure point rather than actually penetrating it. Based on these arguments, the heating time t_h defined previously gives a reasonable indication of engagement times and concomitant tracking requirements for laser-weapon systems.

A. Nondimensionalization Approach

Target heating times depend on many variables, including material properties and thickness, beam parameters, and flow conditions. Ideally, the computed solutions can be collapsed into simple relationships between nondimensional groupings of these variables that reflect the essential physics of the problem. The approach taken in this study was to nondimensionalize the computed solutions using the parameters for the thermally thin analytical solution, shown in Eq. (3). This approach is physically justified by the fact that, due to

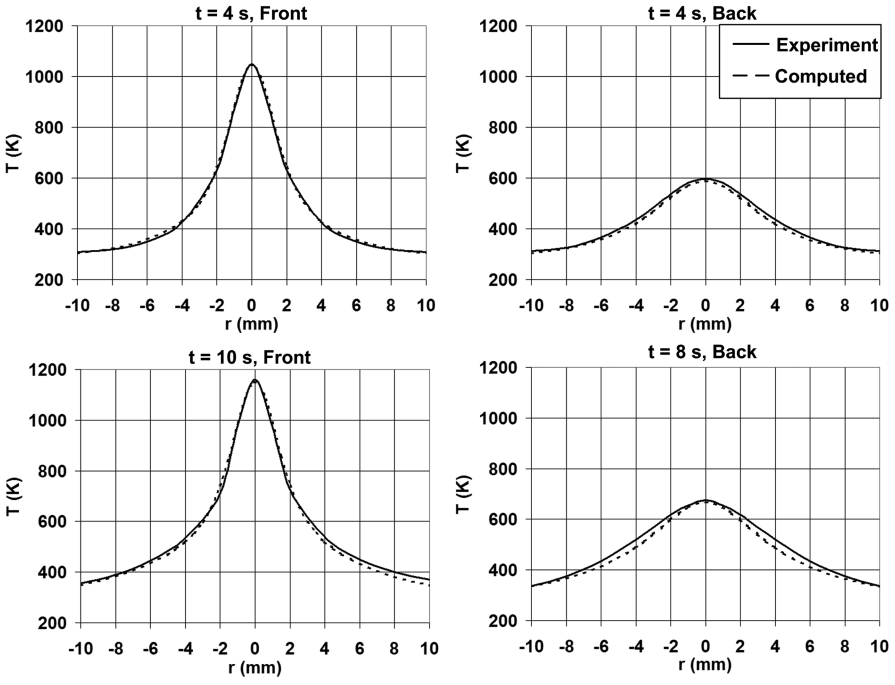

Fig. 4 Measured [6] and computed wind-off temperature distributions on front and back of target plate, $I_0 = 1289$ W/cm^2.

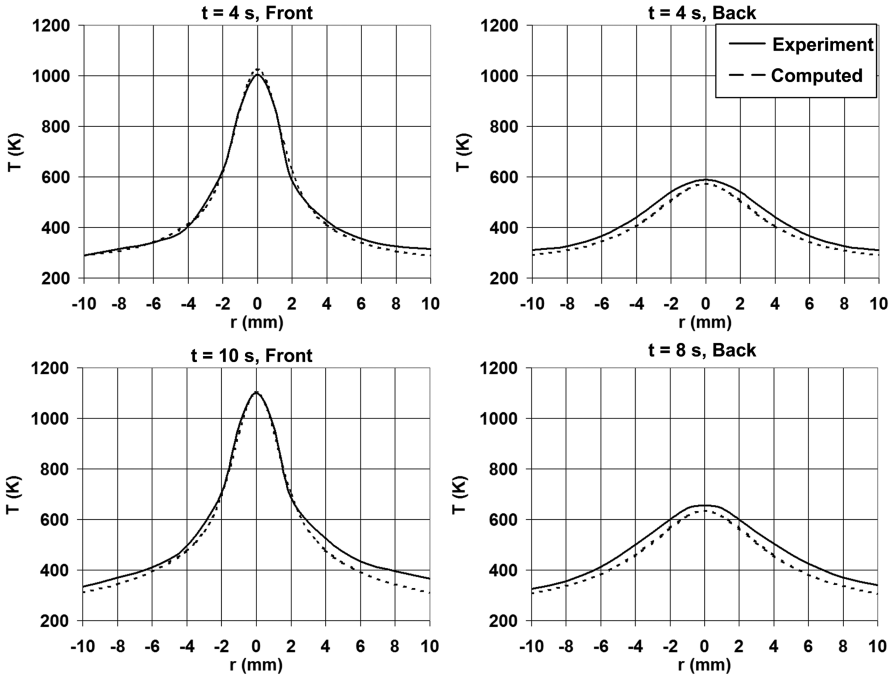

Fig. 5 Measured [6] and computed wind-on ($M = 3.75$) temperature distributions on front and back of target plate, $I_0 = 1289$ W/cm^2.

the small areas of heated surface exposed to the flow and relatively small convective-heat-transfer coefficients, heat transfer by convection can be expected to be small for the laser–target interactions under consideration. As a result, the effect of convective heat transfer on target heating times should be greatest for cases in which the beam irradiance is fairly low (that is, in which the thermally thin solution is most applicable).

Based on the previous discussion, heating times computed using the numerical approach detailed in Sec. II are plotted in Fig. 9 using the nondimensional parameters in Eq. (3). The data shown in Fig. 9 were computed for typical aerospace materials and thicknesses (Table 1). The range of absorbed power and spot sizes used to generate the data are representative of the diffraction-limited performance for contemporary systems at engagement ranges of a few hundred kilometers and emitting at a 1 μm wavelength [3,4,16]; the effective spot size could also be increased due to aiming jitter or the need to induce damage over areas larger than the spot size in order to achieve target failure. For this first use of the nondimensional parameters, the data shown in Fig. 9 were all computed with no

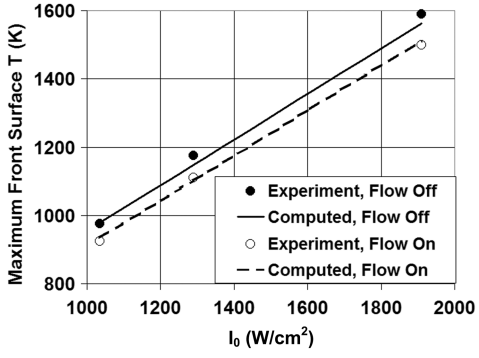

Fig. 6 Measured [6] and computed peak front-surface temperatures.

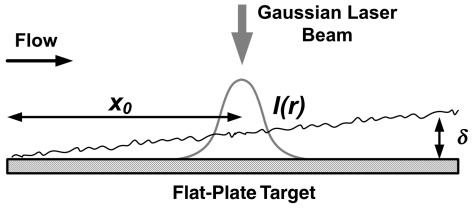

Fig. 7 Schematic of laser–target interaction used in computational study.

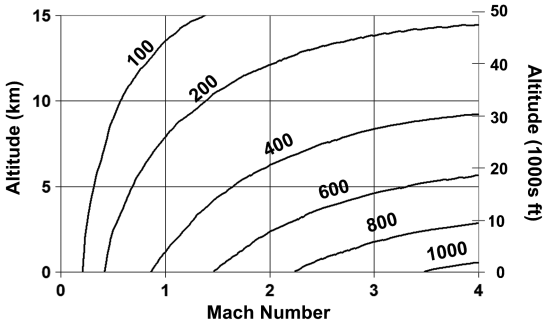

Fig. 8 Variation of convective-heat-transfer coefficient h(W/m^2 K) over the operating envelope of the study.

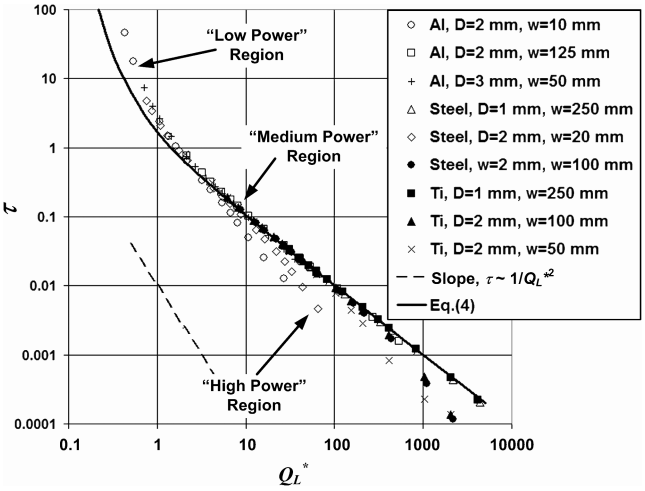

Fig. 9 Computed wind-off heating times nondimensionalized using Eq. (3). For all cases, the material starting temperature T_0 was 290 K.

Table 1 Material properties used for heating time calculations [9]

	Aluminum	AISI-304 stainless steel	Titanium
ρ(kg/m^3))	2698	7900	4500
k(W/mK)	230	25.3	22.7
C_P(J/kg · K)	1083	608	709
Melting temperature, K	933	1730	1988

convective heat transfer. The analytical solution in Eq. (4) is included in the figure for comparison.

Figure 9 clearly shows three distinctive types of behavior in the nondimensionalized numerically computed results. At the left of the figure, the nondimensional heating times τ become increasingly large as $Q_L^* \to 0$; this part of the figure is denoted as the low-power region and corresponds to cases in which the heat input by the laser is nearly balanced by radial conductive heat transfer away from the laser spot. In the center of the figure, the numerical data collapse onto a single curve around $\tau = 1/Q_L^*$; this part of the figure is denoted as the medium-power region for which, as indicated by Eq. (7), the primary effect of the laser is to heat the material directly under the beam. In the low- and medium-power regions, the numerical results precisely match the behaviors predicted by the analytical solutions in Eqs. (5), (6), and (11); this outcome, and the fact that the nondimensional parameters [Eq. (3)] successfully collapse the numerical results onto a single curve in these regions, confirm that the thermally thin model successfully captures the most essential physics of the full numerical code at low and medium powers.

Figure 9 shows that the numerical results also compare well with the analytical solution [Eq. (4)] (solid line) in the low- and medium-power regions, except that the transition between low- and medium-power behavior occurs at a higher nondimensional power for the numerical results. Based on the discussion presented in Sec. II, this higher-power transition associated with the numerical results implies that radial conductive heat transfer remains important at higher powers when the effect of longitudinal heat transfer through the material thickness is included. This outcome is likely due to the fact that the temperature difference through the sheet thickness leads to significantly higher temperatures on the side of the target facing the laser (see, for example, Figs. 4 and 5), resulting in significantly larger radial temperature gradients and concomitantly larger radial conductive heat transfer.

Below the medium-power region in Fig. 9 is a high-power region in which the numerical data diverge from the $\tau \sim 1/Q_L^*$ curve and transition to a $1/Q_L^{*^2}$ trend. The data in this high-power region do not collapse onto a single curve, because the nondimensional parameters [Eq. (3)] are not appropriate for this region. However, the $1/Q_L^{*^2}$ behavior of the data in this region is clearly shown by comparison with the $1/Q_L^{*^2}$-sloped line segment included in the figure (dashed). This $1/Q_L^{*^2}$ trend matches the prediction of Eq. (13) and shows that the heat transfer in this region has transitioned to a slab-heating type of behavior. As shown in [12], high-power behavior occurs when the target thickness exceeds a critical thickness given by

$$D_{\text{crit}} = \frac{0.685\pi w^2 k(T_m - T_0)}{Q_L} \tag{23}$$

Equation (23) has been modified from the original form in [12] to account for a Gaussian irradiance distribution; it accurately predicts the initial transition of the data shown in Fig. 9 from the medium- to the high-power regions.

B. Effect of Convective Heat Transfer

Target heating times with convective-heat-transfer effects included were next computed using the numerical method. Based on the success in collapsing the wind-off data shown in Fig. 9, the wind-on results were also nondimensionalized using the parameters in Eq. (3). As a first test of the wind-on nondimensionalization approach, results were first computed for constant values of the convective-heat-transfer coefficient h; this permitted precise determination of the value of the nondimensional parameter σ for comparison with the analytical solution [Eq. (2)]. Furthermore, the analytical solution [Eq. (2)] assumes convective heat transfer on both sides of the thin plate; as such, the convective-heat-transfer coefficients used in the numerical method were also divided by two before computing the nondimensional parameter σ to compare with the analytical solution.

Computed nondimensional heating times with constant h are shown in Fig. 10 for three different values of the parameter σ, equal to 1, 10, and 100; the figure shows that the nondimensional parameters of Eq. (3) continue to successfully collapse the numerical results when convective-heat-transfer effects are included. Figure 10 shows that the general effect of convective heat transfer is to shift the transition to low-power steady-state-like behavior to higher laser powers, with the power at which this transition occurs increasing with the nondimensional factor σ. This shift in the heating time curves reflects the additional heat removal by convective heat transfer, so that longer heating times are required as the effect of convective heat transfer increases. Figure 10 also shows that the numerical results transition to steady-state-like behavior at slightly higher nondimensional powers than the analytical solution; this can be attributed to the fact that the full numerical solution includes longitudinal heat transfer and, therefore, has higher surface temperatures on the side of the target facing the flow, resulting in greater convective heat transfer.

Although useful for direct comparison of the numerical method with the analytical solution, the constant h results shown in Fig. 10 are not realistic, due to the fact that [as shown by Eqs. (16–20)] the actual convective-heat-transfer coefficient changes significantly as the target surface temperature increases. Figure 11 shows numerical results for variable h computed for realistic flight conditions over the defined study envelope. The data were computed for two different types of wall conditions consisting of hot-wall cases, in which the initial target material temperature was set equal to the flow recovery temperature, and cold-wall cases, in which the initial target temperature was set to the standard-atmosphere sea-level temperature. For these realistic convective-heat-transfer cases, there is some ambiguity in the value of σ, because h can vary considerably during the heating of the target. After some trial and error, it was found that the best collapse of the numerical results was obtained when σ was computed using the value of h at the highest target temperature for each case (i.e., the melting temperature); this approach can be justified, because convective heat transfer is most significant when the target temperature is greatest. Figure 11 shows that the nondimensionalized numerical data still collapse, even for realistic treatment of convective heat transfer; however, the data are slightly more scattered due to the approximate method of determining the parameter σ.

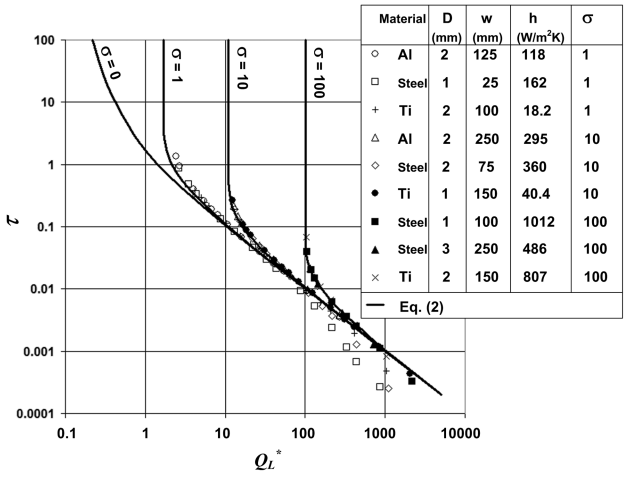

Fig. 10 Heating times computed using numerical method and constant convective-heat-transfer coefficient h. In all cases, $T_0 = 290$ K.

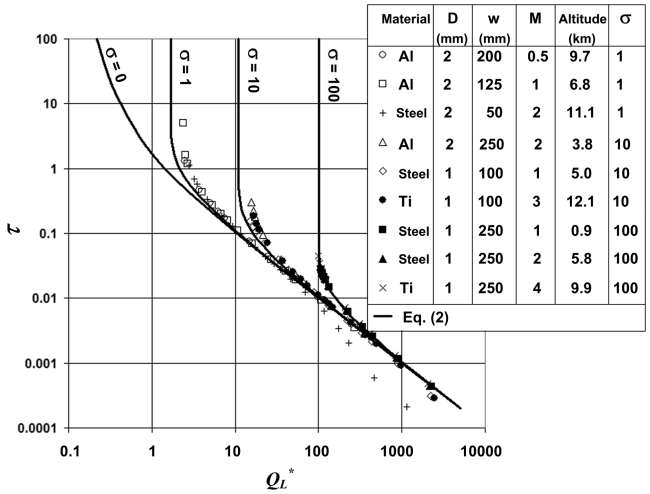

Fig. 11 Computed heating times for realistic convective heat transfer. The parameter σ was computed using the convective-heat-transfer coefficient at the material melting temperature. Material initial temperature was T_r except for final two cases, where T_0 was 290 K.

C. Discussion

The successful collapse of the convective heat transfer results from the full numerical method [shown in Figs. 10 and 11]; using the nondimensional parameters of Eq. (3) demonstrates that the thermally thin approximation captures the essential physics for laser heating of thin materials in realistic flight conditions. This result does not imply that target thickness does not affect realistic laser–target interactions; rather, the essential point is that cases in which the target thickness dominates the heating of the material require such high laser irradiances to heat the target that the effect of convective heat transfer can be safely ignored. As shown by Figs. 10 and 11, convective heat transfer most significantly impacts laser–target interactions in the medium-power region where $\tau \sim 1/Q_L^*$, and the effect of the additional heat removal by convection is to increase heating times and hasten the transition of the laser–target interaction to a steady-state-like behavior. In this medium-power region, the main effect of longitudinal heat transfer through the target material is to establish a temperature variation through the material thickness, so that the side of the target facing the flow is significantly hotter than in the analytical solution; this means that convective heat transfer and radial heat conduction remain important at slightly higher nondimensional powers than indicated by the analytical solution, resulting in a slight shift of the behavior of the full numerical solution to higher Q_L^* when compared with the analytical solution.

Inspection of Figs. 10 and 11 shows that convective-heat-transfer effects become increasingly important as the nondimensional laser power approaches the value of σ. An analysis of Eq. (2) and the numerical results shows that convective heat transfer has less than a 5% effect on heating times if

$$Q_L^* \gtrsim 10\sigma \tag{24}$$

Equation (24) can be used as a simple check for whether convective heat transfer will have a significant effect on the heating time for a given laser–target interaction.

Nondimensionalization of the numerical data and comparison with analytical solutions therefore reveal the manner in which convective heat transfer affects the laser–target interaction for realistic flight conditions; however, Figs. 10 and 11 fail to impart a feel for actual heating times associated with the computed results. Figures 12 and 13 show dimensional heating times as a function of laser power for two cases, one in which $\sigma = 1$ (Fig. 12) and one in which $\sigma = 100$ (Fig. 13); these cases are also plotted in nondimensional form in Figs. 9 and 11. The character of the data shown in Figs. 12 and 13 is best understood by first considering the nondimensional parameter σ, which is approximately the ratio of convective heat transfer over the laser spot area (which is proportional to w^2) to conduction through the material of thickness D under the laser spot. This means that large values of σ can be obtained not only by increasing the convective-heat-transfer coefficient h but also by increasing the size of the laser spot when compared with the target thickness. In fact, studies such as [3–5] indicate that many engagement scenarios occur over a fairly limited range of altitudes and Mach numbers and, therefore, a limited range of h, so that large variations in the nondimensional parameter σ are likely to be caused, at least partially, by variations in spot size and target thickness in addition to variations in h.

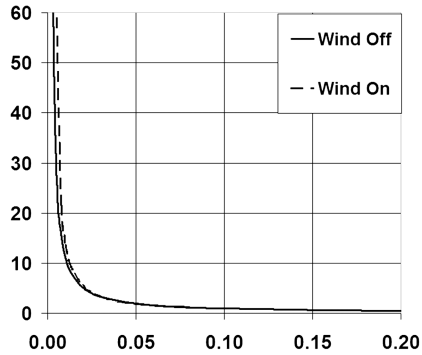

Fig. 12 Dimensional heating times as a function of absorbed laser power for 2-mm-thick aluminum target heated by $w = 125$ mm spot. Wind-on condition is $M = 1$, altitude of 6.8 km, and $\sigma = 1$.

For small values of σ, Eq. (3) shows that, in addition to smaller h, the laser spot diameter w is also relatively small, whereas the material thickness D is relatively large; these conditions cause the heating time to be very sensitive to the input laser power. This sensitivity to laser power is clearly evident in Fig. 12, in which the heating time changes significantly over a change of only a few hundred watts of laser power. As such, the main effect of convective heat transfer is to shift the heating time to asymptotically large times at just marginally higher laser powers, showing that, for small σ, convective heat transfer only has a significant effect on heating times for cases in which the laser power is barely sufficient in the first place.

At large σ, Fig. 13 shows that convective heat transfer noticeably affects the heating time over a much larger range of absorbed laser powers, and up to much higher powers. In particular, the large spot sizes associated with large σ mean that target heating times are already fairly large, even in the wind-off case, so that the increased convective heat transfer associated with large σ is more likely to prolong the target heating to times that may be prohibitively long in terms of tracking the target; this result serves to further emphasize the importance of not just maximizing the power but also minimizing the beam radius on target (i.e., maximizing target irradiance). Further, the contrast in the shapes of the dimensional heating-time curves shown in Figs. 12 and 13 is particularly important if it is noted that larger values of σ (i.e., large spot diameters and small target thicknesses) may be more representative of realistic engagement

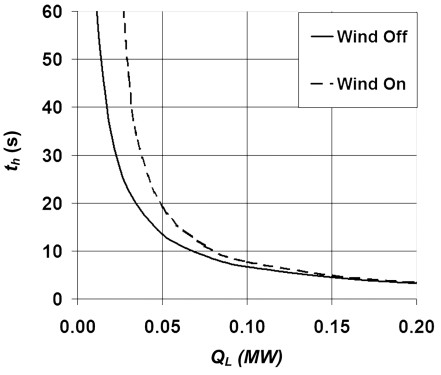

Fig. 13 Dimensional heating times as a function of absorbed laser power for 1-mm-thick stainless-steel target heated by $w = 250$ mm spot. Wind-on condition is $M = 2$, altitude of 5.8 km, and $\sigma = 100$.

scenarios for current systems; for example, engagement parameters given in [3] for heating of a generic missile by a system similar to the Airborne Laser give values of σ up to 1000. In these cases of high σ, convective heat transfer can be expected to significantly affect target heating times at higher laser powers and over a greater range of laser powers.

IV. Conclusions

In summary, the results of this numerical investigation show that convective heat transfer can be expected to significantly affect heating times for laser–target interactions in which the value of the nondimensional parameter σ is large. Convective heat transfer will not be a significant factor for laser–target interaction cases in which the material thickness is greater than the critical thickness, given in Eq. (23). Otherwise, Figs. 10 and 11 show that convective heat transfer has less than a 5% effect on target heating times if $Q_L^* \gtrsim 10\sigma$.

References

[1] Robin, J. E., and Nordin, P., "Reduction of CW Laser Melt-Through Times in Solid Materials by Transverse Gas Flow," *Journal of Applied Physics*, Vol. 46, No. 6, 1975, pp. 2538–2543. doi:10.1063/1.321930

[2] Steen, W. M., *Laser Material Processing*, Springer–Verlag, New York, 1991.

[3] Forden, G. E., "The Airborne Laser," *IEEE Spectrum*, Vol. 34, No. 9, Sept. 1997, pp. 40–49. doi:10.1109/6.619379

[4] Horkovitch, J. A., "Directed Energy Weapons: Promise and Reality," AIAA Paper 2006-3753, June 2006.

[5] Duffner, R. W., *Airborne Laser: Bullets of Light*, Plenum, New York, 1997.

[6] Marineau, E. C., Schetz, J. A., and Neel, R. E., "Computational and Experimental Investigation of Supersonic Convection over a Laser Heated Target," *Journal of Thermophysics and Heat Transfer*, Vol. 23, No. 3, 2009, pp. 502–512. doi:10.2514/1.33697

[7] Carslaw, H. S., and Jaeger, J. C., *Conduction of Heat in Solids*, 2nd ed., Clarendon, Oxford, 1959.

[8] Ready, J. F., *Effects of High-Power Laser Radiation*, Academic Press, New York, 1971.

[9] Wigglesworth, R. G., "A Numerical Model of Surface Recession Phenomena of Metals Subjected to Laser Radiation in an Aerodynamic Environment," M.S. Thesis, Air Force Inst. of Technology, GAW/MC/72-17, Wright-Patterson AFB, OH, Dec. 1972.

[10] Torvik, P. J., "Thermal Response Calculations and Their Role in the Design of Experiments," Air Force Inst. of Technology TR 73-6, Wright-Patterson AFB, OH, Dec. 1973.

[11] Marineau, E. C., Schetz, J. A., and Neel, R. E., "Turbulent Navier–Stokes Simulations of Heat Transfer with Complex Wall Temperature Variations," *Journal of Thermophysics and Heat Transfer*, Vol. 21, No. 3, 2007, pp. 525–535. doi:10.2514/1.26007

[12] Shulstad, R. A., "Laser Induced Heating: Prediction of Front Surface Melting Times," *Air Force Academy Aeronautics Digest*, U.S. Air Force Academy TR 78-6, 1978, pp. 93–99.

[13] Croft, D. R., and Lilley, D. G., *Heat Transfer Calculations Using Finite Difference Equations*, Applied Science Publishers, London, 1977.

[14] Eckert, E. R. G., "Engineering Relations for Heat Transfer and Friction in High-Velocity Laminar and Turbulent Boundary-Layer Flow Over Surfaces With Constant Pressure and Temperature," *Transactions of the ASME*, Vol. 78, Aug. 1956, pp. 1273–1283.

[15] White, F. M., *Viscous Fluid Flow*, 2nd ed., McGraw–Hill, New York, 1991.

[16] Pines, D. (ed.), "Report to The American Physical Society of the Study Group on Science and Technology of Directed Energy Weapons," *Reviews of Modern Physics*, Vol. 59, No. 3, Part 2, 1987, Paper S1-S202. doi:10.1103/RevModPhys.59.S1